Theor Chem Acc (2011) 130:1085–1093
DOI 10.1007/s00214-011-1018-5

REGULAR ARTICLE

Thermodynamic aspects of fibroblastic spreading on diamond-like carbon films containing titanium dioxide nanoparticles

F. R. Marciano · C. C. Wachesk · A. O. Lobo · V. J. Trava-Airoldi · C. Pacheco-Soares · N. S. Da-Silva

Received: 4 April 2011 / Accepted: 8 August 2011 / Published online: 10 September 2011

Abstract The combination of low friction, wear resistance, high hardness, biocompatibility, and chemical inertness makes diamond-like carbon (DLC) films suitable in numerous applications in biomedical engineering. The cytotoxicity of DLC films containing TiO_2 nanoparticles was practical and theoretically evaluated. The films were grown on 316L stainless steel substrates from a dispersion of TiO_2 nanopowder in hexane. Raman spectroscopy shows that the presence of TiO_2 increased the graphite-like bonds in the films. The incorporation of TiO_2 nanoparticles into DLC films increases surface roughness, decreases water contact angle (increased hydrophilic character), and increases the total free surface energy due to the higher polar component. As the concentration of TiO_2 increased, the films increased the cell viability (MTT assay), becoming more thermodynamically favorable to cell spreading (ΔF_{Adh} values became more negative). This was evidenced through the increasing number of projections (philopodia and lamellipodia), indicating a higher adhesion between the L929 cells and the films. The practical and theoretical findings of this study show that the incorporation of TiO_2 into DLC films is effective in enhancing cell viability. These results show the potential use of DLC and TiO_2-DLC films in biomedical applications.

Keywords Diamond-like carbon · TiO_2 nanoparticles · Cellular viability · Work of adhesion · Hydrophilicity · Cell spreading

Dedicated to Professor Akira Imamura on the occasion of his 77th birthday and published as part of the Imamura Festschrift Issue.

F. R. Marciano (✉) · A. O. Lobo
Laboratorio de Nanotecnologia Biomedica (NanoBio),
Universidade do Vale do Paraiba (Univap),
Av. Shishima Hifumi 2911, Sao Jose dos Campos,
SP 12244-000, Brazil
e-mail: femarciano@uol.com.br

C. C. Wachesk · C. Pacheco-Soares · N. S. Da-Silva
Laboratório de Biologia Celular e Tecidual,
Universidade do Vale do Paraiba (Univap),
Av. Shishima Hifumi 2911, Sao Jose dos Campos,
SP 12244-000, Brazil

V. J. Trava-Airoldi
Laboratório Associado de Sensores e Materiais (LAS),
Instituto Nacional de Pesquisas Espaciais (INPE),
Av. dos Astronautas 1758, Sao Jose dos Campos,
SP 12227-010, Brazil

1 Introduction

Surfaces play a vital role in biology and medicine with most biological reactions occurring on surfaces and at interfaces [1]. The successful incorporation of an implant into the body depends on tissue integration and infection resistance, which is influenced by the adherence of autologous cells and bacteria to the surfaces [1, 2]. Cell adhesion and spreading is fundamentally essential for biomaterials that are frequently used in biomedical devices [3]. In most cases, a surface modification of these biomaterials is considered a prerequisite for improving biocompatibility, because this kind of material should also be hard, wear resistant, with a low friction coefficient, and corrosion resistant for certain applications [4].

Diamond-like carbon (DLC) coatings have been actively studied over the last decade in the field of material engineering. Consisting of dense amorphous carbon or hydrocarbon, the mechanical properties of the DLC films fall between those of graphite and diamond [5–8]. These coatings can also impart wear resistance, hardness, and

corrosion resistance to the surface of a medical device and have been considered for use in a variety of cardiovascular, orthopedic, biosensor, and implantable microelectromechanical system devices [9, 10]. Recent studies have reported modified DLC films improved biocompatibility, lubricity, stability, and cell adhesion [11–14]. According to Yun et al. [11], these characteristics are related to structural bonds [15, 16], surface roughness [17, 18], and whether the film is hydrophobic or hydrophilic [19, 20].

Titanium dioxide (TiO_2) has been widely studied in regard to various electronic applications, utilizing its photocatalytic nature and transparent conductivity, which strongly depend on the crystalline structure, morphology, and crystallite size [21]. Due to TiO_2 photo-semiconductor properties, it may be used as an antibacterial agent for the decomposition of organisms [22, 23].

Thorwarth et al. [24] studied the biocompatible properties of the DLC-TiO_x films on a $TiAl_6V_4$ alloy prepared by the plasma immersion ion implantation and deposition (PIII&D) technique. In vitro biocompatibility tests showed promising results concerning proliferation and differentiation of human osteoblasts for the DLC-TiOx films. Amin et al. [25] synthesized DLC films containing titanium oxide (DLC-TiO_x, $x \leq 2$) using the pulsed DC metal–organic plasma-activated chemical vapor deposition (MOCVD) technique. The biomimetic growth of amorphous carbonated apatite on the DLC-TiOx in simulated body fluid (SBF) was found to be dependent on the Ti content of the film.

Our previous publication reported for the first time the production and characterization of TiO_2-DLC films using plasma-enhanced chemical vapor deposition (PECVD) [26]. The method used permits the incorporation of TiO_2 nanoparticles into the film structure during the deposition process. The results demonstrated that these films are potential antibacterial agents with the increasing concentration of TiO_2 nanoparticles. However, it is very important to evaluate the cellular behavior of this new biomaterial.

This paper investigates the cytotoxicity and cell adhesion on DLC films containing TiO_2 nanoparticles. The cell spreading behavior was evaluated using physicochemical properties.

2 Materials and Methods

The 316L stainless steel (SS) substrates (1×1 cm^2) were mechanically polished to a mirror-like finished surface, cleaned ultrasonically in an acetone bath for 15 min, and dried in nitrogen atmosphere. The clean samples were mounted on a water-cooled, 10-cm-diameter cathode, which was powered by a pulsed direct current plasma-enhanced chemical vapor deposition power supply, with variable pulse voltage from 0 to −1,000 V, at a frequency of 20 kHz and duty cycle of 50%.

In the chamber (vacuum base pressure of 1.3 mPa), the substrates were additionally cleaned by argon discharge with 1 sccm gas flow at 11.3 Pa working pressure and a discharge voltage of −700 V for 10 min prior to deposition. In order to enhance the DLC film adhesion to metallic surfaces, a thin amorphous silicon interlayer (thickness around 200 nm) was deposited using silane as the precursor gas (1 sccm gas flow at 11.3 Pa for 12 min and a discharge voltage of −700 V) [27]. The DLC films were deposited using hexane as the feed gas to a thickness of around 2.0 μm (at 18.0 Pa for 60 min and a discharge voltage of −700 V).

In order to produce TiO_2-DLC films, TiO_2 nanoparticles (Aeroxide® TiO_2 P25 from Evonik), in anatase crystalline form with average particle size of 21 nm, were dispersed in hexane at 0.1, 0.5, and 1.0 g/L. These dispersions replaced the pure hexane during the DLC deposition. Figure 1 shows the schematic of the deposition setup, where (a) is the deposition chamber, (b) is the valve, and (c) is the compartment where hexane or hexane dispersion of TiO_2 nanoparticles was inserted into the chamber. In order to perform the deposition of TiO_2-DLC films, the valve (b) opens to allow the hexane to enter into the chamber.

The atomic arrangement of the films was analyzed by Raman scattering spectroscopy by using a Renishaw 2000 system with an Ar^+-ion laser ($\lambda = 514$ nm) in backscattering geometry. The laser power on the sample was ~0.6 mW, and the laser spot was 2.5 μm in diameter. The Raman shift was calibrated in relation to the diamond peak

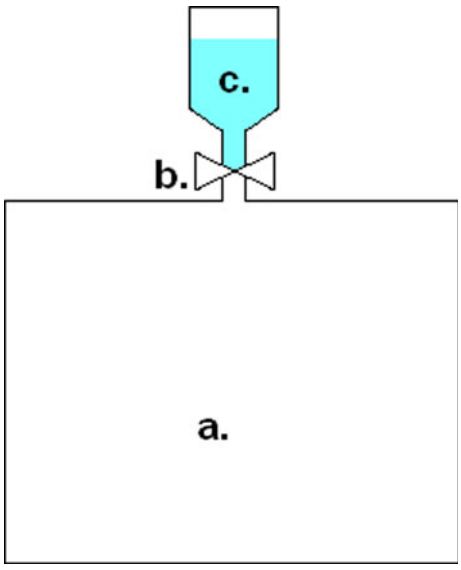

Fig. 1 Schematic of the deposition setup: **a** is dedeposition chamber, **b** is the valve and **c** is the compartment where hexane or hexane dispersion of TiO_2 nanoparticles were inserted into the chamber

at 1,332 cm^{-1}. All measurements were taken in air at room temperature.

The film roughness values were characterized using atomic force microscopy (AFM), VEECO Multimode V, operating in dynamic mode, with 0.01-0.025 Ohm-cm Antimony (n) doped Si tip (model TESPW).

Mouse fibroblast cells (L-929) were provided by Cell Line Bank of Rio de Janeiro/Brazil (CR019). The cells were maintained as subconfluent monolayers in a minimum essential medium (MEM) with 1.5 mM L-glutamine adjusted to contain 2.2 g/L sodium bicarbonate 85%, fetal bovine serum (FBS) 15% (Gibco, BRL), 100 units/ml penicillin–streptomycin (Sigma), and 25 μg/mL l-ascorbic acid (Sigma). The incubation occurred in a CO_2 (5%) atmosphere at 37 °C.

The cytotoxicity assay was evaluated according to ISO 10993-5 "Biological evaluation of medical devices—Test for cytotoxicity: in vitro methods" (or EN 30993-5), using direct contact. The proliferative activity of cultured cells was determined with MTT colorimetric assay, as described by Mosmann [28]. Latex fragments were used as positive control. Fragments of filter paper to prove the nontoxic nature were used as negative control. The dimensions of these fragments were the same as the substrates with DLC and TiO_2-DLC films. All the samples were sterilized in humid vapor (121 °C, 1 atm) and placed in individual wells of 24-well culture plates. L929 mouse fibroblasts were seeded in each well at a concentration of 5×10^5 cells/mL, supplemented with 10% fetal bovine serum (Gibco, BRL). The incubation was performed under a CO_2 (5%) atmosphere at 37 °C for 24 h. After the incubation, the substrates with DLC and TiO_2-DLC films as well as the positive and negative control fragments were removed from their respective wells. Only the cells that adhered to the well walls were incubated with a tetrazolium salt solution (MTT) 3-[4,5-dimethylthiazol-2-yl]-2,5-diphenyltetrazolium bromide (Sigma, St. Louis, MO, USA), at 37 °C for 4 h. The MTT was reduced to an insoluble formazan precipitate by the mitochondrial succinic dehydrogenase of the viable cells. After removal of the medium, ethanol–dimethyl sulfoxide (DMSO) (Sigma) solution (1:1) was added to each well. After complete solubilization of the dark blue crystal of MTT formazan, the absorbance of the content of each well was measured at 570 nm with a 24-well microplate reader on a spectrophotometer Spectra Count (Packard). The blank reference was taken from wells without cells, also incubated with MTT solution. The cell viability was calculated by the normalization of optical densities (OD) to the negative control [29].

The OD were normalized by the negative control and expressed in percentage:

$$[(OD_{sample} - OD_{background})/(OD_{negativecontrol} - OD_{background})] * 100. \quad (1)$$

Data were collected from five different experiments and expressed as the average ± the standard deviation (SD). The statistical differences were analyzed by two-way Anova (Graph Pad Prism 5®). The populations from the DLC and TiO_2-DLC films were obtained with normal distribution and independent to each group of samples. P values less than 0.05 were considered to indicate statistical differences (no data shown).

The capacity of cellular adhesion of the L-929 cells on the DLC and TiO_2-DLC films with different concentrations was evaluated after 24 h. After the incubation, the samples were fixed with a 3% glutaraldehyde (0.1 M) sodium cacodylate buffer for 1 h and dehydrated in a graded ethanol solution series (30, 50, 70, 95, 100%) for 10 min each. The drying stage used a 1:1 solution of ethanol with hexamethyldisilazane (HMDS), and the samples were dried with pure HMDS at room temperature. After deposition of a thin gold layer, the cell spreading on the samples was examined by scanning electron microscopy (SEM—ZEISS EVO MA10).

The contact angle (θ) of the samples was measured by using the sessile drop method with a Kruss EasyDrop contact angle instrument (EasyDrop DSA 100). Two different test liquids (distilled water and diiodomethane) were used for surface energy calculations, according to the Owens method [30]. The liquid was dropped automatically by a computer-controlled system. All measurements were taken at room temperature.

The surface energy composed of polar and dispersive components of the samples was evaluated by measuring contact angle. The interfacial tension between two condensed phases can be determined by Young' equation [31], according to which

$$\cos\theta\gamma_{LV} = \gamma_{SV} - \gamma_{SL}, \quad (2)$$

where θ is the measured contact angle between liquid and solid, and γ_{LV}, γ_{SV}, and γ_{SL} are the interfacial energies of the liquid/vapor, solid/vapor, and solid/liquid interfaces, respectively. This equation can be rewritten as the Young-Duprè equation:

$$W_a = \gamma_{LV}(1 + \cos\theta) = \gamma_{SV} - \gamma_{SL}, \quad (3)$$

where W_a is the adhesion energy per unit area of the solid and liquid surfaces. In the general form of Eqs. (2), (3) then can be written:

$$\gamma_{LV}(1 + \cos\theta) = 2\sqrt{\gamma_L^p \gamma_S^p} + 2\sqrt{\gamma_L^D \gamma_S^D}, \quad (4)$$

where γ_L^p and γ_S^p are the polar components of the surface energy of liquid and solid phases, respectively, and γ_L^D and

Table 1 Test liquids and their surface tension components [32]

Surface tension data (mN/m)	γ_L^D	γ_L^p	γ_{LV}
Water	21.8	51.0	72.8
Diiodomethane	50.8	0.0	50.8

γ_S^D are the dispersive component of the surface energy of the liquid and solid phases, respectively. Because γ_L^D and γ_L^p have been published for many liquids, it is possible to approximate γ_L^D and γ_S^p from a single measurement of θ by using equation (4). Therefore, by measuring the contact angles of two different liquids (distilled water and diiodomethane) with well-known polar and dispersive components of surface energy (Table 1), Eq. (4) can be solved to determine the polar and dispersive components of the surface energy of the materials [32–34]. The liquid was dropped automatically by a computer-controlled system. All measurements were taken at room temperature.

Thermodynamically, the process of adhesion and spreading of cells and bacteria from a liquid suspension onto solid substrata can be described by the following equation [35]:

$$\Delta F_{\mathrm{Adh}} = \gamma_{\mathrm{CS}} - \gamma_{\mathrm{CL}} - \gamma_{\mathrm{SL}}, \tag{5}$$

where ΔF_{Adh} is the interfacial free energy of adhesion, γ_{CS} is the cell-solid substratum interfacial free energy, γ_{CL} the cell-liquid interfacial free energy, and γ_{SL} is the solid–liquid interfacial free energy, respectively. They can be calculated by using contact angle data and the van Oss acid–base approach [36–38].

The following equation was used to determine the interfacial energy of cell adhesion to a solid surface [36–38]:

$$\Delta F_{\mathrm{Adh}} = 2\begin{pmatrix} \sqrt{\gamma_S^{LW}\gamma_L^{LW}} + \sqrt{\gamma_S^p\gamma_L^D} + \sqrt{\gamma_S^D\gamma_L^p} \\ +\sqrt{\gamma_C^{LW}\gamma_L^{LW}} + \sqrt{\gamma_C^p\gamma_L^D} + \sqrt{\gamma_C^D\gamma_L^p} \\ -\sqrt{\gamma_S^{LW}\gamma_C^{LW}} - \sqrt{\gamma_S^p\gamma_C^D} - \sqrt{\gamma_S^D\gamma_C^p} - \gamma_L \end{pmatrix}. \tag{6}$$

According to thermodynamic theory, if ΔF_{Adh} is negative, cell spreading is energetically favorable; while if ΔF_{Adh} is positive, cell spreading is thermodynamically unfavorable.

In order to avoid different UV sources in the contact angle and cell viability measurements, all the experiments were performed using the same light source. In this way, all the differences encountered in the experimental values are regarding only to the different samples (DLC, and TiO_2-DLC in different concentrations of TiO_2).

3 Results and discussions

Raman scattering spectroscopy was used to evaluate the chemical structure of the DLC films. Typical DLC spectra exhibit two distribution bands in the 1,000–1,800 cm^{-1} range, known as the *D* and *G* bands [39]. These spectra were fitted using two Gaussian curves. The integrated intensity ratio of the *D* and *G* peaks (I_D/I_G) has been correlated with the sp^3/sp^2 bonding ratio [40, 41]. In amorphous material, there is a complete loss of periodicity because the *G* peak comprises all sp^2 sites, but the *D* peak only comprises sixfold rings. Therefore, I_D/I_G falls as the number of rings per cluster and the fraction of chain groups rise [42]. Figure 2 shows the spectra from DLC film and from DLC containing TiO_2 nanoparticles at different concentrations, which are vertically shifted for easy comparison. Table 2 summarizes the main characteristics of these Raman spectra. The main factor affecting band position, width, and intensity is the clustering of sp^2 phase [43]. The full width at half maximum of the *G* band FWHM(*G*) and *G* band position both measure disorder; however, FWHM(*G*) is mainly sensitive to structural disorder, while the *G* band position is mainly sensitive to topological disorder [44]. Structural disorder arises from bond angle and bond length distortions [44]. Topological disorder arises from the size and shape distribution of sp^2 clusters [44]. The incorporation of TiO_2 nanoparticles into DLC films results in the increase in the intensity ratio of *D* and *G* peak (I_D/I_G) and a shifting of *D* and *G* bands toward higher wave numbers. These characteristics imply the increase of the graphite-like bonds in DLC matrix [5]. TiO_2-DLC samples have a third band arising from TiO_2

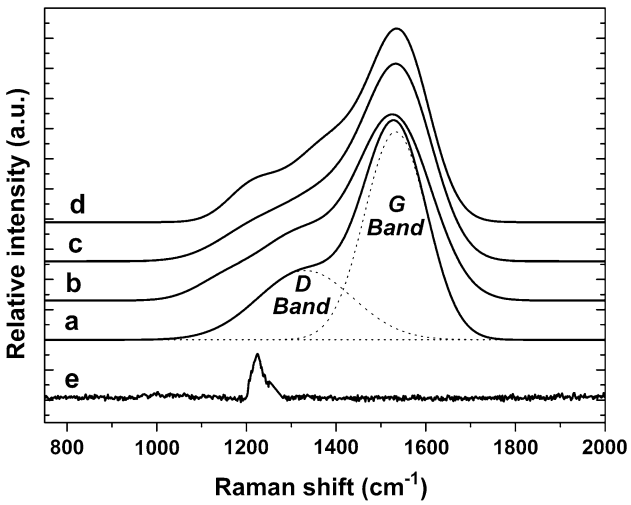

Fig. 2 Raman scattering spectra from **a** DLC film; DLC containing TiO_2 nanoparticles in the concentration of **b** 0.1, **c** 0.5, and **d** 1.0 g/L [27]; and **e** TiO_2 powder. The spectra are vertically shifted for easy comparison

Table 2 Gaussian fitting results of Raman spectra from DLC films with various TiO_2 concentrations [26]

TiO_2 concentration (g/L)	*D* band position (cm^{-1})	*G* band position (cm^{-1})	TiO_2 band position (cm^{-1})	FWHM (*G*)	I_D/I_G
0.0	1,328.5	1,534.1	–	168.4	1.35
0.1	1,347.5	1,538.1	1,201.8	161.9	1.37
0.5	1,377.2	1,542.4	1,189.3	162.0	1.39
1.0	1,380.3	1,543.0	1,158.6	176.2	1.48

Table 3 Average roughness of DLC films with different TiO_2 concentrations. Each mean value corresponds to the average value on three different areas

TiO_2 concentration (g/L)	Average roughness (nm)
0.0	4.7 ± 0.5
0.1	5.9 ± 0.8
0.5	6.8 ± 0.7
1.0	7.0 ± 0.5

nanoparticles. The TiO_2 powder spectrum shows a band at 1,226.0 cm^{-1} (Fig. 2e). When the concentration of TiO_2 nanoparticles in DLC films increased, the TiO_2 band shifts toward TiO_2 powder peak.

The surface roughness measured through AFM images over an area of 1 μm x 1 μm can be seen on Table 3. Even though all the surfaces are considerably smooth, the presence of TiO_2 nanoparticles in DLC films slightly increased their surface roughness. More details regarding DLC and TiO_2-DLC films can be seen in a previous manuscript [26].

The cell viability is positively correlated with the degree of MTT reduction [28, 34, 45]. Figure 3 shows the cell viability found for DLC and TiO_2-DLC films, compared to the negative and positive controls. The positive control has very low cell viability, characterizing cell death. A high index of cell viability is shown for DLC and TiO_2-DLC films. Compared to the positive control, the DLC and TiO_2-DLC films are evidently nontoxic. The increasing concentration of TiO_2 nanoparticles in DLC films enhances the cell viability on these samples.

The adhesion of cells to a surface is determined by the interplay of electrostatic and hydrophobic/hydrophilic interactions [46]. The contact angles of the samples formed with distilled water and diiodomethane are shown in Table 4. As the concentration of TiO_2 nanoparticles in DLC films increased, the water contact angle decreased from 82 to ~50°, and in the case of diiodomethane, the contact angle remained almost constant ~40°. These results are illustrated in Fig. 4. Usually, a hydrophobic surface has a contact angle higher than 70°, while a hydrophilic surface has a contact angle lower than 70° [33]. These results indicate that TiO_2-DLC is hydrophilic and TiO_2-DLC films acquired the hydrophilic characteristic from the amorphous TiO_2 surfaces [47].

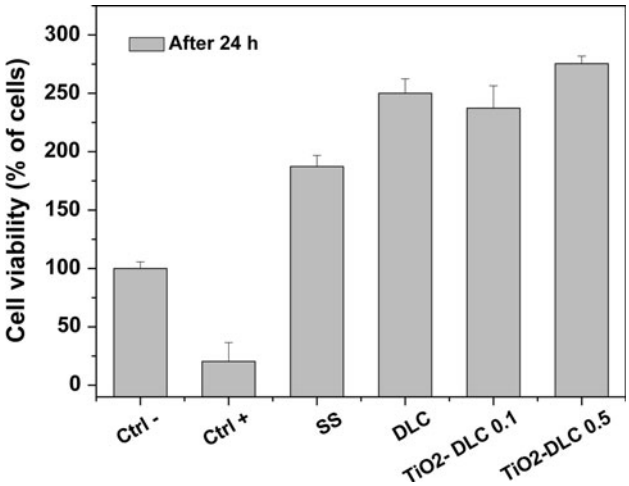

Fig. 3 L929 mouse fibroblasts viability curve measured by MTT assay

Table 4 Contact angle of DLC and TiO_2-DLC films with different TiO_2 concentrations

TiO_2 concentration (g/L)	Contact angle, θ (°)	
	Water	Diiodomethane
0.0	82.3 ± 4.5	40.2 ± 1.6
0.1	53.0 ± 2.1	39.6 ± 2.4
0.5	53.3 ± 1.5	44.1 ± 5.4
1.0	49.0 ± 2.2	39.6 ± 2.4

Each mean value corresponds to the average value on five different areas

Some researchers have reported that cell adhesion appears to be maximized on moderately wettable surfaces with water contact angles in the range of 60–90° [48–51]. The DLC and TiO_2-DLC water contact angle values in this range are independent of TiO_2 nanoparticle concentration. However, van Wachem et al. [49], who studied human endothelial cells, further suggest that moderately wettable surfaces increase the adsorption of serum proteins, which thereby increases cell attachment, spreading, and adhesion. In this case, the TiO_2-DLC films will be more applicable.

The water contact angle is an important property of a cell culture substrate. Another important property directly related to it is the surface free energy of the substrate,

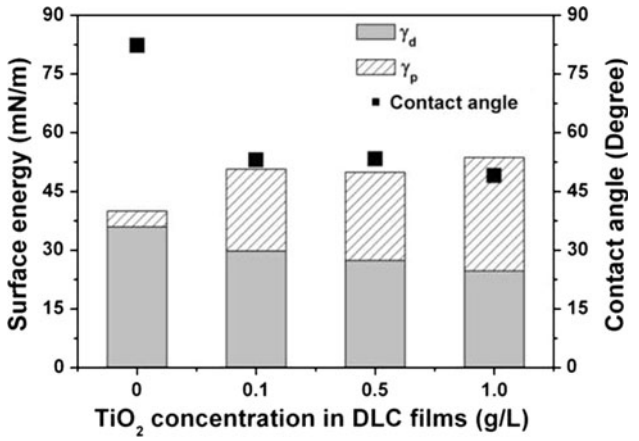

Fig. 4 Dependence of the water contact angle and the surface energy of TiO_2-DLC samples according to the TiO_2 concentration in the films

Table 5 Surface energy components of DLC and TiO_2-DLC films with different TiO_2 concentrations

TiO_2 concentration (g/L)	Surface free energy (mN/m)			$\gamma_p/(\gamma_d + \gamma_p)$
	Dispersive (γ_d)	Polar (γ_p)	Total	
0.0	36.0	4.0	40.0	0.10
0.1	29.8	20.9	50.7	0.41
0.5	27.4	22.5	49.9	0.45
1.0	24.7	29.0	53.7	0.54

Each mean value corresponds to the average value on five different areas

which has been shown to be related to the function of tissue cultured on the substrate, including attachment, spreading, and growth [48].

The surface energy components obtained according to the Owens method [30] are also listed in Table 5. The total surface energy (γ) of 40.0 mN/m for the as-deposited DLC films is estimated as the sum of a dispersive component ($\gamma_d = 36.0$ mN/m) and a polar component ($\gamma_p = 4.0$ mN/m). The interfacial free energy determines the wetting characteristics, and hence, the wall shear stress generated when the liquid comes into contact with the surface [30]. As the concentration of TiO_2 nanoparticles in DLC films increased, the total surface energy also increased from 40.0 to 53.7 mN/m. The increase in the total surface energy of TiO_2-DLC films is attributed to the increase in the polar component. TiO_2-DLC films have a higher polar component due to the oxide particles on the surface [52]. The polar components attract the electric dipoles of water, which minimizes the interfacial energy and the water contact angle [52]. The water contact angle decreased as the polar component in the surface energy increased. Electric dipole of water molecule is attracted by the polar component, which reduces the interfacial energy between the surface and the water, and thus, the wetting angle of water [53].

The influence of the polar and dispersive components on fibroblast adhesion has been previously reported for different polymeric biomaterials [54, 55]. Hallab et al. [55] studied the correlation between biomaterial surface energy and directed cell adhesion. They stated that while the polar component of the surface free energy seemed to be an accurate determinant of cellular adhesion, a poor correlation was observed for the dispersive component [55]. The fractional polarity [3] (FP $= \gamma_p/(\gamma_d + \gamma_p)$) has been previously correlated with cell attachment and cell spreading [55]. Hallab et al. [55] stated that the shear strength of cell adhesion reached its maximum at around 0.5 FP. In the present study, films containing 0.5 and 1.0 g/L of TiO_2 are in this range.

A thermodynamic approach offers a powerful tool to predict cell spreading to solid substrates [34, 45]. For this, the surface free energy values of L929 mouse fibroblasts (γ_C) calculated by Schakenraad et al. [35] were used. The average values of work of adhesion (ΔF_{Adh}) for the studied samples are listed in Table 6. All the calculated values for ΔF_{Adh} for L929 mouse fibroblast adhesion on DLC and TiO_2-DLC films are negative ($\Delta F_{Adh} < 0$). As provided by Schakenraad et al. [35], a negative value for ΔF_{Adh} indicates conditions that are favorable for cell adhesion. In addition, as the TiO_2 concentration increases in DLC films, the ΔF_{Adh} values became more negative. This result suggests that as the TiO_2 content in DLC films increased, they became more thermodynamically favorable to cell spreading.

The theoretical results were compared to SEM images from the studied samples. Figure 5 shows the SEM images of L-929 cells morphology totally spreading on (a) DLC, (b) 0.1 g/L TiO_2-DLC, and (c) 0.5 g/L TiO_2-DLC films. The very healthy cell behavior was observed in both substrates (DLC and TiO_2-DLC films). The SEM images clearly show cells with a higher number of membrane projections on TiO_2-DLC (Fig. 4b, c) films compared to DLC (Fig. 5a) films. Figure 5a illustrates cell spreading on DLC films. L929 are flattened over DLC surface, extending their philopodia (arrows) and lamellipodia (stars) membranes. In Fig. 5b, from 0.1 g/L TiO_2-DLC films, the cells

Table 6 Interfacial free energy of adhesion of DLC and TiO_2-DLC films with different TiO_2 concentrations

TiO_2 Concentration (g/L)	Interfacial free energy of adhesion (mJ/m^2)
0.0	−7.6
0.1	−14.5
0.5	−16.2
1.0	−17.1

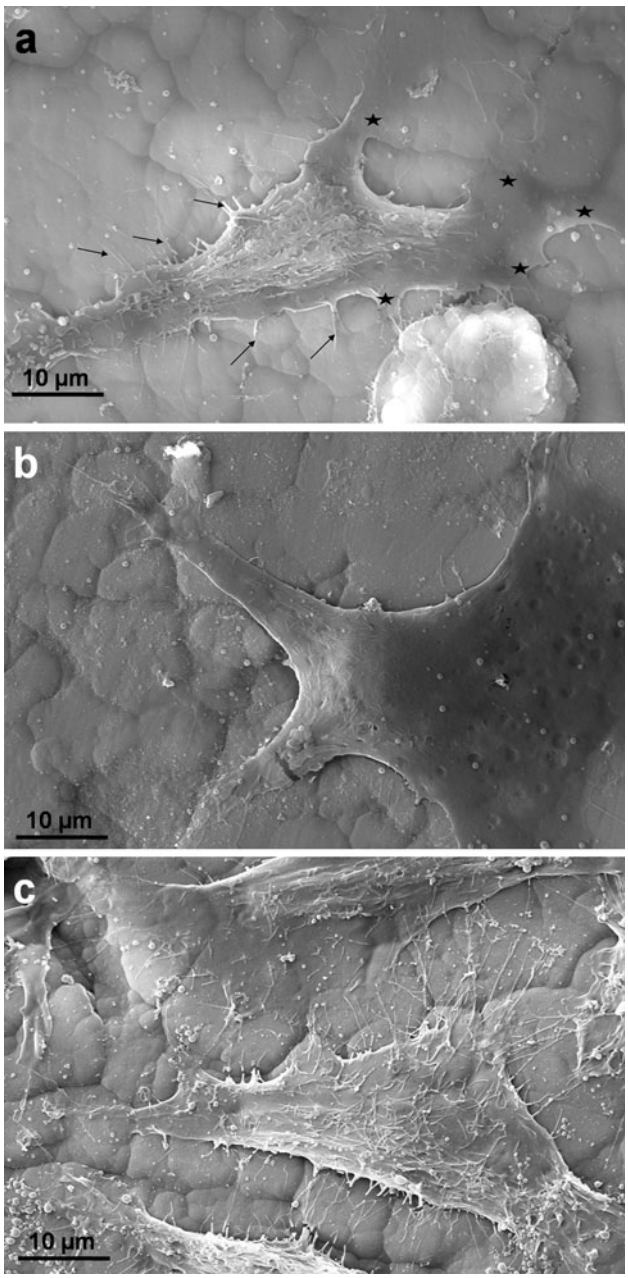

Fig. 5 SEM images of L929 mouse fibroblast spreading on **a** DLC, **b** 0.1 g/L TiO_2-DLC, and **c** 0.5 g/L TiO_2-DLC films

become more flattened and tensioned (high adhesion), with the presence of more lamellipodia. In Fig. 5c, from 0.5 g/L TiO_2-DLC films, L929 cells are completely flattened, with a huge number of extended philopodia and lamellipodia membranes. The increasing number of membrane projections (philopodia and lamellipodia) evidenced the increasing adhesion between L929 cells and DLC films with increasing TiO_2 content.

Cellular adhesion is generally dependent on time, adhesive forces at the cell/material interface, and surface topography. Several authors have shown that an initial period of time (e.g., 6–24 h) is essential for the cell adhesion due to migration and proliferation of the cells on nanobiomaterial surfaces [56, 57]. Fibroblasts play a particularly important role in the wound repair process as one of the first tissues involved with the repair of damaged or diseased tissue. Substrate properties including the water contact angle [48], surface free energy [35], and roughness [48, 58] can influence cellular processes of attachment, spreading, and growth. Furthermore, fibroblast spreading has been correlated with surface free energy, with greatest spreading on substrates with surface free energy greater than 45 (mN/m) [49, 55], as in the case of all the TiO_2-DLC films in this manuscript.

4 Conclusions

In this paper, the spreading of L929 mouse fibroblasts cells was studied by physicochemical properties and thermodynamic approach on diamond-like carbon films containing TiO_2 nanoparticles. Cell viability increases with increasing concentration of TiO_2 in the films. Multiple factors are likely to mediate this enhancement, such as the increasing of the surface roughness, decreasing of water contact angle (increasing of hydrophilic character), and increasing of the total surface free energy due to the higher polar component. In addition, the presence of TiO_2 increased the graphite-like bonds in DLC films. As the concentration of TiO_2 increased, the films become more thermodynamically favorable to cell spreading (ΔF_{Adh} values became more negative), which was evidenced through the increasing number of projections (philopodia and lamellipodia), indicating a higher adhesion between L929 cells and the films. The practical and theoretical findings of this study show that the incorporation of TiO_2 into DLC films was effective in enhancing cell viability.

Acknowledgments This study was supported by Conselho Nacional de Desenvolvimento Científico e Tecnológico (CNPq) and Fundação de Amparo à Pesquisa do Estado de São Paulo (FAPESP).

References

1. Castner DG, Ratner BD (2002) Biomedical surface science: foundations to frontiers. Surf Sci 500:28–60
2. Randeniya LK, Bendavid A, Martin PJ, Amin MS, Rohanizadeh R, Tang F, Cairney JM (2010) Thin-film nanocomposites of diamond-like carbon and titanium oxide; Osteoblast adhesion and surface properties. Diamond Relat Mater 19:329–335
3. Karakeçili AG, Gümüsderelioglu M (2008) Physico-chemical and thermodynamic aspects of fibroblastic attachment on RGDS-modified chitosan membranes. Coll Surf B 61:216–223
4. Chai F, Mathis N, Blanchemain N, Meunier C, Hildebrand HF (2008) Osteoblast interaction with DLC-coated Si substrates. Acta Biomater 4:1369–1381

5. Robertson J (2002) Diamond-like amorphous carbon. Mat Sci Eng R 37:129–281
6. Donnet C, Fontaine J, Le Mogne T, Belin M, Héau C, Terrat JP, Vaux F, Pont G (1999) Diamond-like carbon-based functionally gradient coatings for space tribology. Surf Coat Technol 120–212:548–554
7. Donnet C, Grill A (1997) Friction control of diamond-like carbon coatings. Surf Coat Technol 94–95:456–462
8. Yun DY, Choi WS, Park YS, Hong B (2008) Effect of H_2 and O_2 plasma etching treatment on the surface of diamond-like carbon thin film. Appl Surf Sci 254:7925–7928
9. Shirakura A, Nakaya M, Koga Y, Kodama H, Hasebe T, Suzuki T (2006) Diamond-like carbon films for PET bottles and medical applications. Thin Sol Films 494:84–91
10. Morrison ML, Buchanan RA, Berry LiawPK, CJ BrigmonRL, Riester L, Abernathy H, Jin C, Narayan RJ (2006) Electrochemical and antimicrobial properties of diamondlike carbon-metal composite films. Diamond Relat Mater 15:138–146
11. Uzumaki ET, Lambert CS, Santos AR Jr, Zavaglia CAC (2006) Surface properties and cell behaviour of diamond-like carbon coatings produced by plasma immersion. Thin Sol Films 515:293–300
12. Zhang S, Du H, Ong SE, Aung KN, Too HC, Miao X (2006) Bonding structure and haemocompatibility of silicon-incorporated amorphous carbon. Thin Sol Films 515:66–72
13. Hauert R (2003) A review of modified DLC coatings for biological applications. Diamond Relat Mater 12:583–589
14. Nakamura T, Ohana T, Suzuki M, Ishihara M, Tanaka A, Koga Y (2005) Surface modification of diamond-like carbon films with perfluorooctyl functionalities and their surface properties. Surf Sci 580:101–106
15. Chen JY, Wang LP, Fu KY, Huang N, Leng Y, Leng YX, Yang P, Wang J, Wan GJ, Sun H, Tian XB, Chu PK (2002) Blood compatibility and sp^3/sp^2 contents of diamond-like carbon (DLC) synthesized by plasma immersion ion implantation-deposition. Surf Coat Technol 156:289–294
16. Zhao Q, Liu Y, Wang C, Wang S (2007) Bacterial adhesion on silicon-doped diamond-like carbon films. Diamond Relat Mater 16:1682–1687
17. Ma WJ, Ruys AJ, Mason RS, Martin PJ, Bendavid A, Liu Z, Ionescu M, Zreiqat H (2007) DLC coatings: Effects of physical and chemical properties on biological response. Biomaterials 28:1620–1628
18. McLaughlin JA, Meenan B, Maguire P, Jamieson N (1996) Properties of diamond like carbon thin film coatings on stainless steel medical guidewires. Diamond Relat Mater 5:486–491
19. Yokota T, Terai T, Kobayashi T, Meguro T, Iwaki M (2007) Cell adhesion to nitrogen-doped DLCs fabricated by plasma-based ion implantation and deposition method using toluene gas. Surf Coat Technol 201:8048–8051
20. Rich A, Harris AK (1981) Anomalous preferences of macrophages for roughened and hydrophobic substrata. J Cell Sci 50:1–7
21. Nakano H, Hasuike H, Kisoda K, Nishio K, Isshiki T, Harima H (2009) Synthesis of TiO_2 nanocrystals controlled by means of the size of magnetic elements and the level of doping with them. J Phys Condens Matter 21:064214
22. Huang Z, Maness PC, Blake DM, Wolfrum EJ, Smolinski SL, Jacoby WA (2000) Bactericidal mode of titanium dioxide photocatalysis. J Photochem Photobiol A Chem 130:163–170
23. Shun-Wen W, Bing P, Li-Yuan C, Yun-Chao L, Zhu-Ying L (2008) Preparation of doping titania antibacterial powder by ultrasonic spray pyrolysis. Trans Nonferrous Met Soc China 18:1145–1150
24. Thorwarth G, Saldamli B, Schwarz F, Jürgens P, Leiggener C, Sader R, Haeberlen M, Assmann W, Stritzker B (2007) Biocompatibility of doped diamond-like carbon coatings for medical implants. Plasma Process Polym 4:S364–S368
25. Amin MS, Randeniya LK, Bendavid A, Martin PJ, Preston EW (2009) Amorphous carbonated apatite formation on diamond-like carbon containing titanium oxide. Diamond Relat Mater 18:1139–1144
26. Marciano FR, Lima-Oliveira DA, Da-Silva NS, Diniz AV, Corat EJ, Trava-Airoldi VJ (2009) Antibacterial activity of DLC films containing TiO_2 nanoparticles. J Colloid Interface Sci 340:87–92
27. Bonetti LF, Capote G, Santos LV, Corat EJ, Trava-Airoldi VJ (2006) Adhesion studies of diamond-like carbon films deposited on Ti6Al4V substrate with a silicon interlayer. Thin Solid Films 515:375–379
28. Mosmann T (1983) Rapid colorimetric assay for cellular growth and survival: application to proliferation and cytotoxicity assays. J Immunol Methods 65:55–63
29. Lobo AO, Antunes EF, Machado AHA, Pacheco-Soares C, Trava-Airoldi VJ, Corat EJ (2008) Cell viability and adhesion on as grown multi-wall carbon nanotube films. Mat Sci Eng C 28:264–269
30. Owens DK, Wendt RC (1969) Estimation of the surface free energy of polymers. J Appl Polym Sci 13:1741–1747
31. Young T (1805) An essay on the cohesion of fluids. Philos Trans Roy Soc 95:65–87
32. Van Oss CJ, Good RJ, Chaundhury MK (1986) The role of van der Waals forces and hydrogen bonds in "hydrophobic interactions" between biopolymers and low energy surfaces. J Colloid Interf Sci 111:378–390
33. Choi HW, Dauskardt RH, Lee SC, Lee KR, Oh KH (2008) Characteristic of silver doped DLC films on surface properties and protein adsorption. Diamond Relat Mater 17:252–257
34. Flahaut E, Durrieu MC, Remy-Zolghadri M, Bareille R, Ch Baquey (2006) Investigation of the cytotoxicity of CCVD carbon nanotubes. J Mater Sci 41:2411–2416
35. Schakenraad JM, Busscher HJ, Wildevuur CRH, Arends J (1988) Thermodynamic aspects of cell spreading on solid substrata. Cell Biophys 13:75–91
36. Liu C, Zhao Q, Liu Y, Wang S, Abel EW (2008) Reduction of bacterial adhesion on modified DLC coatings. Colloids Surf B Biointerfaces 61:182–187
37. Schneider RP (1996) Conditioning film-induced modification of substratum physicochemistry—analysis by contact angles. J Colloid Interface Sci 182:204–213
38. Wang J, Huang N, Pan CJ, Kwok SCH, Yang P, Leng YX, Chen JY, Sun H, Wan GJ, Liu ZY, Chu PK (2004) Bacterial repellence from polyethylene terephthalate surface modified by acetylene plasma immersion ion implantation-deposition. Surf Coat Technol 186:299–304
39. Tuinstra F, Koening JF (1970) Raman spectrum of graphite. J Chem Phys 53:1126–1130
40. Dillon O, Woollam J, Katkanant V (1984) Use of Raman-scattering to investigate disorder and crystallite formation in as-deposited and annealed carbon-films. Phys Rev B 29:3482–3489
41. Beeman D, Silvermann J, Lynds R, Anderson MR (1984) Modeling studies of amorphous carbon. Phys Rev B 30:870–875
42. Tamor MA, Vassell WC (1994) Raman fingerprinting of amorphous-carbon films. J Appl Phys 76:3823–3830
43. Casiraghi C, Piazza F, Ferrari AC, Grambole D, Robertson J (2005) Bonding in hydrogenated diamond-like carbon by Raman spectroscopy. Diamond Relat Mater 14:1098–1102
44. Casiraghi C, Ferrari AC, Robertson J (2005) Raman spectroscopy of hydrogenated amorphous carbons. Phys Rev B 72:085401–085414
45. Hussain SM, Hess KL, Gearhart JM, Geiss KT, Schlager JJ (2005) In vitro toxicity of nanoparticles in BRL 3A rat liver cells. Toxicol In Vitro 19:975–983

46. Yao KS, Wang DY, Chang CY, Weng KW, Yang LY, Lee SJ, Cheng TC, Hwang CC (2007) Photocatalytic disinfection of phytopathogenic bacteria by dye-sensitized TiO_2 thin film activated by visible light. Surf Coat Technol 202:1329–1332
47. Sobczyk-Guzenda A, Gazicki-Lipman M, Szymanowski H, Kowalski J, Wojciechowski P, Halamus T, Tracz A (2009) Characterization of thin TiO_2 films prepared by plasma enhanced chemical vapour deposition for optical and photocatalytic applications. Thin Sol Films 517:5409–5414
48. Tamada Y, Ikada Y (1994) Fibroblast growth on polymer surfaces and biosynthesis of collagen. J Biomed Mater Res 28:783–789
49. van Wachem P, Hogt A, Beugeling T, Feijen J, Bantjes A, Detmers J, van Aken W (1987) Adhesion of cultured human endothelial cells onto methacrylate polymers with varying surface wettability and charge. Biomaterials 8:323–328
50. Ikada Y (1994) Surface modification of polymers for medical applications. Biomaterials 15:726–736
51. Hasson J, Wiebe D, Abbott W (1987) Adult human vascular endothelial cell attachment and migration on novel bioabsorbable polymers. Arch Surg 122:428–430
52. Roy PK, Choi HW, Yi JW, Moon MW, Lee KR, Han DK, Shin JH, Kamijo A, Hasebe T (2009) Hemocompatibility of surface-modified, silicon-incorporated, diamond-like carbon films. Acta Biomater 5:249–256
53. Roy RK, Choi HW, Park SJ, Lee KR (2007) Surface energy of the plasma treated Si incorporated diamond-like carbon films. Diamond Relat Mater 16:1732–1738
54. Redey SA, Razzouk S, Rey C, Bernache-Assollant D, Leroy G, Nardin M, Cournot G (1999) Osteoclast adhesion and activity on synthetic hydroxyapatite, carbonated hydroxyapatite, and natural calcium carbonate: relationship to surface energies. J Biomed Mater Res 45:140–147
55. Hallab N, Bundy K, O'Connor K, Moses RL, Jacobs JJ (2001) Evaluation of metallic and polymeric biomaterial surface energy and surface roughness characteristics for directed cell adhesion. Tissue Eng 7:55–71
56. Sniadecki NJ, Desai RA, Ruiz AS, Chen CS (2005) Nanotechnology for cell–substrate interactions. Ann Biomed Eng 34:59–74
57. Thomas V, Dean DR, Vohra YK (2006) Nanostructured Biomaterials for regenerative medicine. Curr Nanosci 2:3155–17757
58. Van der Valk P, Van Pelt AWJ, Busscher HJ, de Jong HP, ChRH Wildevuur, Arends J (1983) Interaction of fibroblasts and polymer surfaces: relationship between surface free energy and fibroblast spreading. J Biomed Mater Res 17:807–817